SCA-9828

STOCHASTIC DESCRIPTION OF EXPERIMENTAL 3D PERMEABILITY FIELDS IN VUGGY RESERVOIR CORES

C.Dauba*, G.Hamon**, M.Quintard*, D. Lasseux*.
* L.E.P.T.ENSAM (UA CNRS), Talence, France.
** Elf Exploration Production, Pau, France.

Abstract

Unsteady-state core waterfloods on vuggy samples often result in early water breakthrough. The interpretation of transient production data frequently leads to anomalous relative permeability curves. This might be attributable to small-scale heterogeneity. To confirm this assumption, 1) the effect on permeability of a single vug within a unit matrix cell was simulated, 2) the quantification of small-scale heterogeneity was carried out on seven long vuggy reservoir cores used for waterflood tests. Finally the comparison between the 3D fields of local permeabilities and global transport properties was performed.

For each vuggy whole-core the following sequence of tasks was performed : 1) A dense probe permeameter data set was gathered, using a 5mm spacing along 24 lines of the core surface. More than 1000 permeability values were approximately obtained for a 20 cm long sample. 2) Experimental semivariograms of local permeability were obtained from the probe data set. 3) Multiple images of 3D permeability fields were generated according to the experimental semivariogram. More than 20000 grid cells were usually populated with permeability for each core sample. 4) Global sample permeability was calculated with a single-phase simulator for each realisation of the 3D core. 5) Experimental and calculated global sample permeability were compared.

The following conclusions were drawn : 1) An isolated vug within a unit matrix cell results in a low increase of permeability. It also means that the distribution of vug diameters has a small effect on overall permeability. Quantification of small-scale heterogeneity should directly focus on permeability distribution rather than porosity. 2) Local permeability histograms are very different from one sample to another. 3) The permeability correlation length ranges from 2 to 7 cm. Using short horizontal plugs rather than long vertical samples might result in sample-spanning high permeability paths and erroneous waterflood results. 4) Comparison between experimental and calculated global sample permeability often shows a good agreement. It confirms that dense surface probe permeameter data is often, but not always, able to capture most of the permeability heterogeneity on vuggy cores.

Introduction

Water/oil relative permeability curves are usually obtained on carefully selected, homogeneous core samples. This is problematic for vuggy reservoirs and the interpretation of unsteady-state corefloods with 1D numerical model or standard JBN interpretation sometimes results in intriguing relative permeabilities. This is confirmed by the few studies devoted to the interpretation of corefloods on vugular samples, [De Zabala & Kamath,1995 ; Erlich, 1971]. Small-scale heterogeneity was claimed to control the flow

behaviour and the most recent studies took advantage of the computed tomography (CT) scanning to characterise porosity and coreflood behaviour [Hicks & al, 1992 ; MacAllister & Miller, 1993].

When large variations in permeability or porosity occur at the sample scale, like in vugular cores, it is not proven that the relative permeability formulation is still valid. Previous studies concluded that the conditions under which the relative permeability formulation is adequate mainly depend on the standard deviation of the permeability distribution and the ratio of the correlation length to the total length [Chang & Mohanty, 1994]. It means that corefloods must be performed on well selected samples in order to be able to extract meaningful relative permeability curves from experimental data. This is particularly important for coreflood experiments using CT scanning and live fluids which are expensive and time consuming. In others words, a priori knowledge of the 3D permeability field would be a good criterion to select the sample to be waterflooded, among all available vuggy samples.

The objective of this paper is to confirm whether a 3D permeability field can be easily obtained for each candidate sample, to be used as an homogeneity criterion prior to coreflood experiments. First, we are documenting why we are not using CT scanning to generate 3D permeability fields. Secondly, experimental 2D permeability fields obtained on vuggy cores with an automated probe permeameter are presented. Stochastic generation of 3D permeability fields is described. Finally, experimental and computed permeability at the core scale are compared.

Effect of Heterogeneity at the vug scale :

Several studies of the effect of small scale heterogeneity on two phase flow behavior of vuggy samples devoted a lot of effort to get the distribution of vug diameters or porosity, through CT scanning for instance [Hicks & al, 1992]. This approach might be misleading as shown hereafter.

In a first step, the modification of intrinsic permeability due to vugs was studied at the vug scale. FLUENT® was used to perform flow simulations on a model porous structure represented by a unit cell made of a porous matrix containing a unique vug (See Figure 1). This software solves general equations for mass, momentum and energy transport on structured or unstructured grids using finite difference schemes. In the present work, a coupled Stokes -in the vug zone- and Darcy -in the matrix zone- model was used. Overall permeability K*, of the unit cell was calculated. Sensitivity to the matrix permeability K_m was carried out. In our calculations, the vug to total cell volume ratio was roughly 20%, the total porosity was 24% while the matrix permeability, K_m, ranged from 1mD to 1D. The resulting overall permeability was found to be linearly dependant of the matrix permeability as $K^* = 1.488^* K_m$.

The coefficient of 1.48 shows that an isolated vug within a unit matrix cell results in a small increase of permeability. In other words, an isolated vug has a low influence on overall permeability, even when the porosity of the unit cell is large. This might also indicate that :

- the histogram of vug diameters is not necessarily a clue of the flow behavior of vugular cores.
- generating 3D permeability maps from CT scan porosity data might not be representative, since vug porosity and overall permeability might not be directly related.

The above observations suggest an alternative approach to get insights into the small scale heterogeneity effects of vugular cores. Rather than measuring 3D local variations of porosity with CT scanning, we tried to get directly 2D local permeability maps from extensive use of an automated probe permeameter and then generate 3D permeability fields constrained by experimental data.

Experimental data acquisition

In this work, seven full size core samples from different Western Africa reservoirs were studied. Six of them are vuggy dolomite while the other one is a limestone. Vug size is of the order of millimeter or centimeter at the most. For all of them, vugs result from fossil fragments dissolution with possible recrystallization and partial filling (see lithological description in Table 1). All samples were cleaned with organic solvents and dried after the completion of coreflood studies.

Table 2 details the geometry and the overall nitrogen permeability of the samples, Kg (Klinkenberg corrected), [Klinkenberg, 1941; Monicard, 1981]. The most immediate observation from the data presented in Table 2 is the low to moderate values of sample permeability : 0.8 to 29 mD, despite the abundance of vugs. It might indicate either that the whole sample is vuggy but individual vugs are not interconnected or that tight non vuggy zones do control the overall permeability.

1- Probe permeameter measurements

An extensive probe permeameter data set was gathered at the surface of each cylindrical sample. Local permeability measurements were performed each 5 mm along 24 generatrices and 24 diameters on end faces (see Figure 2), leading to more than 1000 local permeability values for a 20 cm long sample.

In our experiments, tip seal inner and outer diameters were respectively 3.4 and 7.6 mm featuring a volume investigated by nitrogen of approximately 1 cm^3. The injection flow rate and tip pressure were respectively set to 17.5 ml/min and 7 bars so that the injection pressure could be kept between 0 and 1 bar. When surface roughness or large vug area resulted in a leak at the tip, the permeability value was set automatically at 10 D. Experimental data were interpreted in terms of local permeability by making use of the classical probe permeameter equation which does not include gas slippage correction [Goggin & al.,1988]. It relates the injection pressure, P_1, the ambient pressure, P_2, the gas viscosity, μ, the gas flow rate, Q_1, and the tip inner radius, R_i, to the apparent local permeability, k by :

$$k = \frac{2 * \mu * P_1 * Q_1}{Go^{\infty} * R_i * (P_1^2 - P_2^2)} \qquad (1)$$

In this relationship, G_o^{∞} is a geometric factor which depends on the seal assembly and sample geometry.

The validity of this interpretation was first checked by comparing probe permeameter measurements performed on homogeneous plug faces to their conventional apparent gas permeability. A good agreement was obtained except for samples of permeability lower than 1 mD. In that case, we observe an overestimation by the probe permeameter measurements.

2- Surface permeability map

Once point permeability data had been collected, they were imported into a mapping software to produce iso-permeability maps. Figure 4 highlights high permeability zones reflecting the presence of vugs and low permeability zones also called matrix zones for sample A2. On each core sample, a photographic image was also recorded 360° around the outside of the core. Figures 4 and 5 illustrate the excellent agreement between iso-permeability map and 360° core photography of sample A2. Both images clearly show high permeability vugs clusters at both ends of the core whereas a strip of tight matrix material cuts the middle of the sample. The spatial distribution of the small-scale permeability explains the large difference between very high local permeability values : several Darcies and the low global permeability of about 8.5 mD.

On the other hand, the heterogeneity's spatial distribution of sample A6 is very different. An iso-permeability map of sample A6 (see Figure 3) shows no low permeability zone but a large permeable zone and only a few important vugs. The large permeable zone is made up of hundreds of very small vugs scattered all over the core sample. That results in relatively high overall permeability : 29 mD.

Surface Iso-perm maps are produced for all samples. To accommodate the large variations of local permeability values, the data were contoured using arithmetic or logarithmic values, depending on the sample. This was particularly useful to derive histograms as described in the following section.

3- Histogram of local permeabilities:

Permeability histograms were obtained for each sample. Figures 6 and 7 illustrate the histograms of samples A2 and A6, respectively. At the first glance, both show a large scatter in point permeabilities : from 0.1 to 10000 mD. However, the distribution of local permeabilities are quite different. The A2 sample shows approximately 30% of tight points (between 0.1 and 10 mD) which reflect significant regions with small intergranular permeability. The A2 sample also shows approximately 30% of high perm points (1000-10000mD), suggesting large areas of interconnected vugs. On the other hand, only 15% of the A6 probe data ranges from 0.1 mD to 10 mD, and the permeable zone represents 75% of the data set (10-1000 mD). It is consistent with small vugs spread over a large area and embedded in a porous matrix.

From this observation, it clearly appears that there is no single classical permeability distribution capable of reproducing all experimental data sets.

Another way to specify a permeability distribution is to compute the standard deviation σ_{logk}. Values of σ_{logk} are gathered in Table 2 for each sample. They range between 1.14 and 2.65.

Geostatistical analysis

As a result of sedimentary origins, the distribution of reservoir rocks properties is both random and locally dependent. Our variables are local permeabilities measured at the core surface by the probe permeameter. Geostatistics offers a collection of statistical tools aimed at understanding and modeling spatial variability [Journel, 1989]. First, our purpose is to analyze data spatial correlation thanks to experimental semivariograms, then to draw alternative, equally probable realizations. The results are as many as needed stochastic models of the 3D permeability field constrained by the covariance model.

We have chosen to process experimental data with two methods. With the first one, the method of « corrected logs », we work on the Napierians logarithms of the permeability. In order to avoid any skew, we subtract from each logarithm the average of logs by section.
The second method involves permeability classes. The range of permeability is divided into 5 classes : 0-10 mD, 10-100 mD, 100-1000 mD, 1000-9999 mD and >=10000 mD. We can analyze permeability correlation inside each class.
The core sample is gridded using 20000 cells (regions) $0.343 \cdot 0.343 \cdot 0.5$ cm^3 large. Each cell will be populated with permeability through stochastic simulation.

1- Variogram analysis

The basis of our approach is to link permeability with a distance between pairs of experimental points. In order to describe spatial correlation between permeabilities, we used the semivariogram, $\gamma(\mathbf{h})$, which is defined experimentally by :

$$\gamma(\mathbf{h}) = \frac{1}{2N(\mathbf{h})} \sum (Z(\mathbf{u}+\mathbf{h}) - Z(\mathbf{u}))^2 \qquad (2)$$

Here, $N(\mathbf{h})$ is the number of pairs of points that are separated by the vector distance $\mathbf{h}$ (often referred to as the lag distance) and Z is the variable under consideration, in our case the experimental values of local permeability.
On Figure 8 , four semivariograms of sample A2 are shown. They have been computed from local permeability measurements in horizontal directions, 0° and 90° -both directions are in a cross-section of the core-, in a vertical direction -corresponding to the flow direction- and in all directions -called omnidirectional-. The vertical variogram shows a possible cyclic structure with a period of 4 cm and the correlation length, λ, in that direction, is about 2 cm. On horizontal semivariograms 0 and 90°, no significant anisotropy is observed. From h=4.5 cm, the more ragged appearance of those variograms is probably due to the smaller number of pairs of points available. This makes the determination of a correlation length in the 0° and 90° directions difficult.

Among all information provided by semivariograms, one of the most significant values is the correlation length in the flow direction, i.e. the correlation length of the vertical semivariogram. The vertical correlation length, λ, of each sample is compared to the core length in Table 2. λ ranges from acceptable values for waterflood tests (samples A1, A2 and A3) to very large values : about 40% for samples A4 and A7.

2- Stochastic simulation and 3D permeability fields

Our purpose is to generate equally probable permeability 3D fields, constrained by the experimental covariance (semivariogram) model.
When permeabilities have been transformed into Napierians logarithms (method of « corrected logs »), we compute a sequential Gaussian simulation. This way, we can obtain many stochastic realizations, equally probable and based on the same covariance (semivariogram) model with the method of « corrected logs ».
With the method of « classes », the idea is to discretize the spatial distribution of the continue variable, the local permeability, in 5 classes [Journel & Alabert, 1988]. This process is called sequential indicator simulation and allows to generate many stochastic realizations of 3D permeability field.
The 3D permeability fields can be visualized in 2D longitudinal and cross sections. Two sections in a permeability field of sample A2 are illustrated on Figures 11 and 12 in which experimental points are represented by white crosses.

Calculation of permeability tensor at sample scale

One of the main assumptions of our approach lies behind the representation of 3D permeability fields performed on the basis of 2D surface maps. The fine-scale 3D permeability fields honor the known statistics of each sample but do not give any indication on whether this process was able to capture the 3D physical variations of permeability. A comparison between the global permeability of the sample calculated using fine-scale description and the experimental sample permeability was deemed to be able to bridge the gap.

Several techniques were developed to upscale single phase permeabilities, including harmonic or arithmetic-mean techniques, pressure-solver methods, renormalization techniques and homogenisation theory [Matheron, 1968 ; Bourgeat, 1975 ; Renard & de Marsily, 1997]. In the present work, we used the large-scale averaging method [Quintard & Whitaker, 1987 ; Ahmadi & Quintard, 1995] to compute the large-scale permeability tensor from our Darcy-scale stochastic 3D permeability fields. This fully anisotropic tensor is obtained as the solution of a closure problem described in Quintard & Whitaker (1987) using a finite difference numerical model.

The fine-scale 3D permeability field consisted of 25000 regions. The porosity of each region was set equal to the global core porosity. As shown in 2D surface maps, the permeability contrast between two adjacent regions can exceed several orders of magnitude. For this reason, and to avoid biasing the computation of the equivalent large-scale permeability, each region was subdivided into eight cells. A no-outflow boundary conditions was taken on the outer surface of the sample. The comparison between the computed large-scale permeability and the experimental global one is made on the diagonal term, Kzz, that corresponds to the flow direction. Cross terms are also reported in Table 2.

1- Comparison between simulated and experimental overall permeability

For each sample, several 3D permeability realizations were generated from the same semivariogram model. For all realizations, the global sample permeability was calculated. Figure 9 shows eleven realizations of the computed permeability for sample A5. The

average is 0.42 mD with a standard deviation of 0.06. The same results are presented for sample A1. Figure 10 illustrates twenty equally probable simulations. The average permeability is 25.1 mD and the standard deviation 6.73.
All experimental and simulated results concerning the 7 core samples are gathered in the Table 2. For samples A5, A7, A2 and A6 (Kg are respectively 0.58, 3.9, 8.5 and 29 mD), the estimation obtained by simulation is quite satisfactory : the simulated global permeability is very close to the experimental global one, whatever the method we use. This confirms that 3D permeability fields generated from 2D surface maps have correctly captured small-scale heterogeneity.
On the one hand, the simulated values obtained on sample A1 -18 to 31 mD- (see Figure 10) strongly overestimates the actual global permeability, 1.6 mD. This might be partly explained by the fact that, for this sample, 30% of the measurements produced a permeability value of 10000mD, suggesting leaks often occurred in the probe permeability measurement due to large vugs -1 to 5 mm in this sample.
On the other hand, the simulated permeability of samples A4 and A3 is very low compared to the experimental (see Table 2). 2D surface maps indicate a series flow along the axis of the sample : a low permeability zone sandwiched between vuggy zones of high permeability. The low permeability zone is preponderant and very tight : 70% of probe permeameter values are below 2mD for both samples. This explains the simulated permeability value about 0.05 mD.
It might suggest that preferential paths exist inside the core but they haven't been captured by 2D measurements. To verify this assumption, we performed miscible displacement on sample A3.

2- Miscible displacement

Figure 13 is a plot of effluent concentration of brine as a function of pore volume produced for sample A3 with a constant stepwise variation of brine concentration at the inlet. It reveals one fast path that results in early tracer breakthrough. The experimental curve also displays a long tail effect due to one slow zone in parallel. This behavior is more consistent with parallel flow than series flow. For this sample, it confirms our doubts about not having captured the spatial repartition of small-scale heterogeneity (see above).
Miscible displacements are currently carried out on all samples to be compared with information coming from 2D probe permeameter maps.

Discussion

Probe permeameter measurements on sample A1 show many 10000 mD values. This default maximum value reveals a gas leak, probably due to large vug diameters. Since there is a very poor agreement between experimental and computed permeability values -1.6 mD and 25 mD respectively-, experimental valuation may be improved by modifying of the experimental device, when the vug diameter exceeds 5 mm.
Despite recognized limitations of permeability spatial distribution conveyed by 2D surface maps, significant information has been obtained and particularly about the spatial organization of vug clusters. On two/thirds of samples, 2D surface maps allow the determination of small-scale heterogeneity that is consistent with large-scale permeability.

Comparison between experimental and calculated permeability is a recommended check to ensure that small scale is correctly captured.

The vertical correlation length λ and the standard deviation σ_{logk} are very useful information drawn from permeability fields. Previous studies indicated that the relative permeability formulation may not be adequate when the correlation length is above 20% and especially when the standard deviation σ_{logk} is above 0.2 [Chang & Mohanty, 1994]. Taking into account our results, only sample A6 appears adequate for relative permeability measurements.

It should be kept in mind that experimental data were obtained on long full size samples. However, in the industry, core waterfloods are routinely carried out on small and short core plugs. The above figures of correlation lengths do indicate that using short horizontal plugs rather than long vertical samples might result in sample-spanning high permeability paths and erroneous waterflood results.

The following approach is suggested for the selection of vuggy samples to be used for waterflooding experiments :

- carry out extensive probe permeameter measurements on full size cores as received at the laboratory site.
- estimate correlation lengths per core section.
- cut full size core samples according to the ratio between correlation length and total sample length.
- generate 3D permeability maps, calculate overall permeability.
- perform an miscible flood if a major discrepancy is observed.

Conclusion

The following conclusions were drawn :

1) An isolated vug within a unit matrix cell results in a small increase of permeability. It is confirmed that quantification of small-scale heterogeneity in vuggy rocks should directly focus on permeability distribution rather than porosity or distribution of vug diameters.

2) Local permeability histograms are very different from one sample to another.

3) Comparison between experimental and calculated global sample permeability often shows a good agreement. It confirms that dense surface probe permeameter data is often, but not always, able to capture most of the permeability heterogeneity on vuggy cores.

4) The permeability correlation length ranges from 2 to 7 cm. This may indicate that short plugs should be avoided for waterflood experiments.

Acknowledgments

We are especially grateful to François Petit, Didier Lasseux, Fabien Cherblanc, Pierre Coudin, Pascal Maurin and Alain Dutouya for their help. We would also like to thank Elf Exploration Production and Total for permission to publish this work.

Nomenclature

Cnorm =effluent normalized concentration
Go^{∞} = geometrical factor
h = distance vector, L
k = local permeability
K* = equivalent permeability of flow simulations on a vuggy unit cell
Kg = overall nitrogen permeability
k_m = matrix permeability
Kzz = simulated permeability in the flow direction
N = number of points, dimensionless
P = pressure.
Q = flow rate
R_i = inner tip seal radius, L
S = fluid saturation
T = number of classes
u = location vector, L
PV = pore volume
x,y,z= directions
Z = random variable

Subscripts

o = oil
w = water
1 = inlet
2 = outlet

Greek letters

μ = gas viscosity (cP)
$\gamma(h)$ = semivariogram, fraction^2
σ_{logk} = standard deviation of permeability distribution
λ = correlation length of permeability distribution in the flow direction.

References

Ahmadi, A., Quintard, M., « Large-Scale Properties for Two-Phase Flow in Random Porous Media », *Journal of Hydrology*, (1996), vol. **183**, 69-99.

Bourgeat A., « Global Behavior of Two-Phase Flows in Inhomogeneous Media », *Proceedings 3rd International Conference on Boundary layers*, (1975), Boole Press Publ., Dublin, , 157-160.

Chang Y.C., Mohanty K.K, « Stochastic Description of multiphase Flow in Heterogeneous Reservoirs », *SPE 28443*, 69th ATCE of SPE, New Orleans, USA, Sep. 25-28, 1994.

DeZabala, E.F, Kamath, J., « Laboratory Evaluation of Waterflood Behavior of Vugular Carbonates », *SPE 30780*, ATCE of SPE, Dallas, USA, Oct. 22-25, 1995.

Erlich R., « Relative Permeability Characteristics of Vugular Cores, Their Measurement and Significance », *SPE 3553*, 46th Annual Fall Meeting of the SPE of AIME, New Orleans, USA, Oct. 3-6, 1971.

Goggin D.J., Thrasher R., Lake L.W., « A Theoretical and Experimental Analysis of Minipermeameter Response Including Gas Slippage and High Velocity Effects ». *In Situ*, (1988), vol **12**, 79-116.

Hicks, P.J., Deans, H.A., Narayanan K.R., « Distribution of Residual Oil in Heterogeneous Carbonate Cores Using X Ray CT », *SPEFE*, Sept. 1992, 235-240.

Journel A.G. *Fundamentals of Geostatistics in Five Lessons*, American Geophysical Union, Washington D.C., 1989, 39, Vol. **8** Short Course in Geology.

Journel A.G., Alabert F.G., « Focusing on Spatial Connectivity of Extreme-Valued Attributes : Stochastic Indicator Models of Reservoir Heterogeneities ». *SPE 18324*, 63rd ATCE of SPE, Houston, USA, Oct. 2-5, 1988, 621-632.

Klinkenberg L.J « The Permeability of Porous Media to Liquids and Gases ». *API Drilling and Production Practice*, (1941), 200-213.

MacAllister D.J., Miller K.C., « Application of X-Ray CT Scanning to Determine Gas/Water Relative Permeabilities », *SFEFE*, Sept. 1993, 184-188.
Matheron G., « Composition des Perméabilités en Milieu Poreux Hétérogène : Critique de la Règle de Pondération Géométrique ». *Rev. De l'Inst. Fr. du Pétrole*, (1968), vol. **2**, 201-218.
Monicard R., *Caractéristiques des Roches Réservoirs . Analyse des carottes* , Inst. Fr. du Pétrole, Rueil Malmaison, 1975, 203.
Quintard M., Whitaker S., « Ecoulement Monophasique en Milieu Poreux : Effet des Hétérogénéités Hocales », *Journal de Mécanique théorique et appliquée*, (1987), Vol. **6**, N° 5, 691-726.
Renard Ph., de Marsily G., « Calculating equivalent permeability : a review ». *Water Resour. Res*., (1997), vol **20**, Nos 5-6, , 253-278.

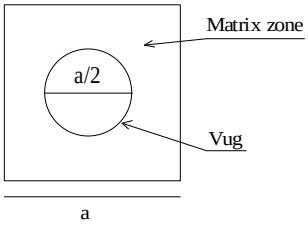

Figure 1 - Geometry of a vugular unit cell for flow simulations.

Core sample	Lithological description
A1	Vuggy dolomicrosparite (no filling).
A2	Vuggy sandy dolomicrosparite (partial filling), vugs <3mm except a few about 1 cm.
A3	Sandy dolosparite (many vugs < 1mm).
A4	2 facies : sandy dolomite and dolomitic sandstone.
A5	Vuggy silt dolomite.
A6	Vuggy dolomite, many microfissures.
A7	Vuggy limestone.

Table 1-Lithological description of the core samples.

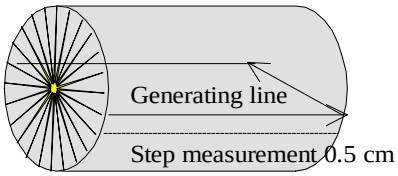

Figure 2 - Probe permeability measurements on core sample.

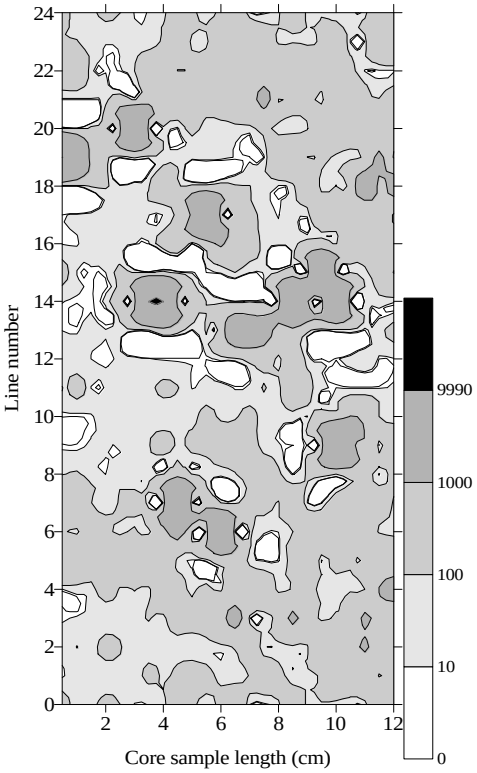

Figure 3 - Surface map of the sample A6 (permeability scale in mD).

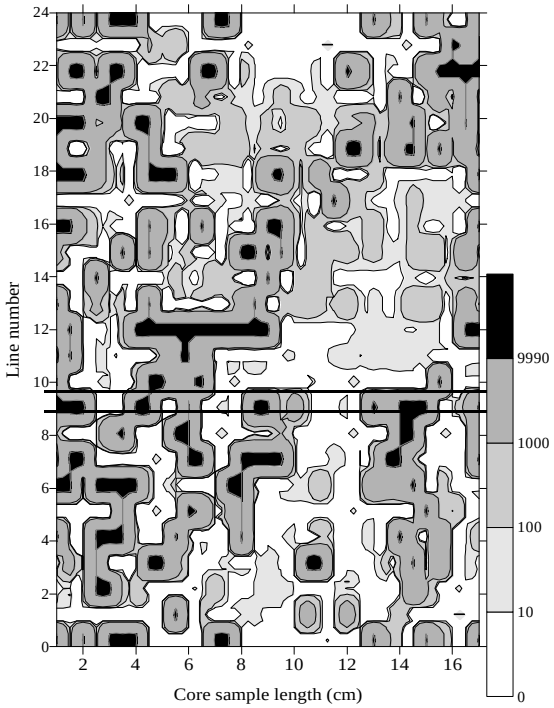

Figure 4 - Surface map of the sample A2 (permeability scale in mD).

Figure 5 - 360° core photography of sample A2.

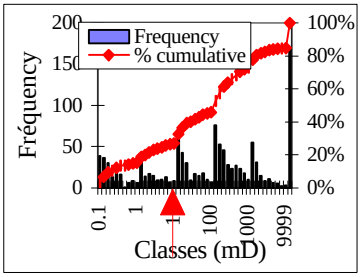

Figure 6 - Distribution histogram of the sample A2 Kg = 8.5 mD.

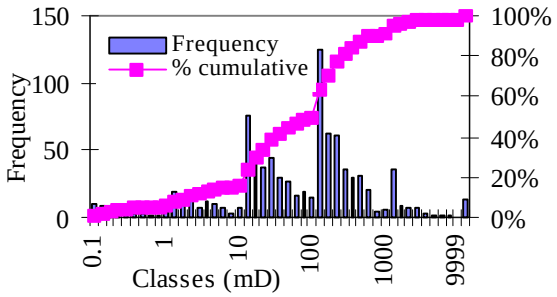

Figure 7 - Distribution histogram of the sample A6 Kg = 29 mD.

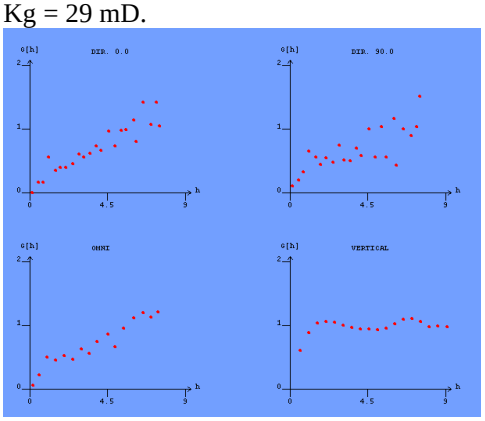

Figure 8 - Semi-variograms of the sample A2 : horizontal 0° et 90°, omnidirectionnal and vertical.

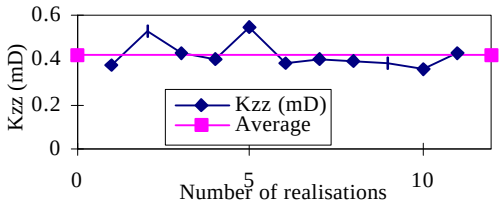

Figure 9 - Spreading of 11 stochastic simulations of the A5 sample (« corrected logs » method).

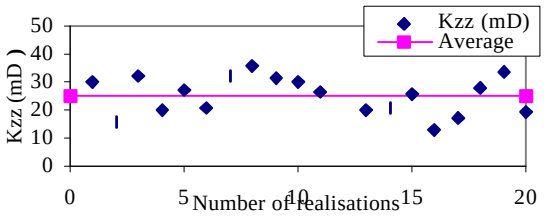

Figure 10 - Spreading of 20 stochastic simulations of the A1 sample (« corrected logs » method).

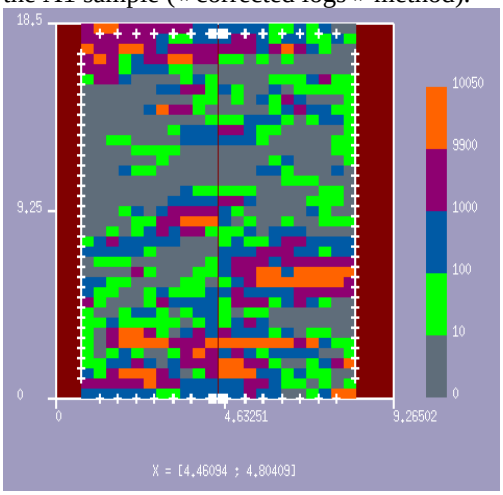

Figure 11 - Longitudinal section along the X axis of 3D permeability field of the sample A2.

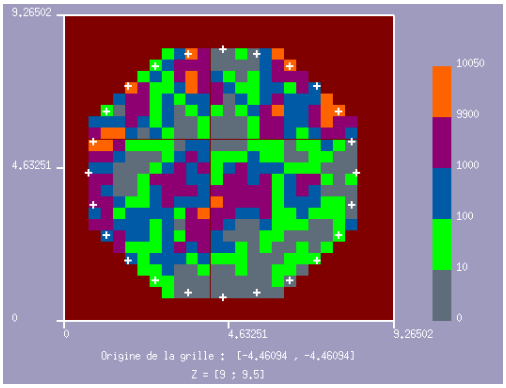

Figure 12 - Cross section along the Z axis of 3D permeability field of the sample A2.

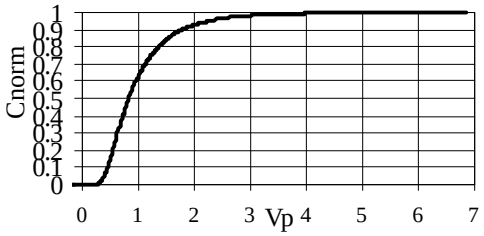

Figure 13 - Experimental tracer dispersion curve showing the variation of the normalized density of the fluid at the outlet of sample A3.

Core sample	**A1**	**A2**	**A3**	**A4**	**A5**	**A 6**	**A 7**
Diameter (cm)	7.5	7.5	7.5	7.5	7.5	7.5	7.5
Length (cm)	14.7	19	28.6	15.7	19	12.6	21.6
Porosity (%)	20.1	18.8	14.2	12.4	19.6	22.5	15
Kg (mD)	**1.6**	**8.5**	**4.6**	**0.8**	**0.58**	**29**	**3.9**
λ (cm)	2.7	2	5	7	4.5	3.5	9
Ratio (%) : λ / total length	18	10.5	17.5	43.7	23.7	27.7	41.6
σ_{logk}	2.65	1.83	1.36	1.38	1.88	1.14	2.58
Cell size (dx·dy·dz in cm)	0.343·0.343·0.5						
Cells number of the simulated 3D field (nx·ny·nz)	27·27·31 22599 regions	27·27·37 26973 regions	27·27·59 43011 regions	27·27·33 24057 regions	27·27·39 28431 regions	27·27·26 18954 regions	27·27·44 32076 regions
Cells number for the single phase flow model (nx·ny·nz)	54·54·62	54·54·74	27·27·59	54·54·66	54·54·78	54·54·52	54·54·88
Permeability tensor (mD)	**method of « corrected logs »**						
kxx kyy	0.045 0.05	0.0008 0.0006	0.0001 0.0002	0.0001 0.0001	0.008 0.015	-0 -0	N/A
kzz	**25.13**	**6.2**	**0.044**	**0.03**	**0.42**	**28.01**	
kyx kzx kzy	0.184 -0.001 -0.017	-0.018 -0.022 -0.008	-0.0007 -0.00004 0.00001	0.0003 0.0003 -0.0002	0.010 0.005 -0.010	-0 0 -0	
Permeability tensor (mD)	**method of « classes »**						
kxx kyy	0.037 0.047	0.036 0.0348	0.0088 0.0055	0.002 0.005	0.004 0.003	0. 0	0.007115 0.0065
kzz	**12.44**	**6.48**	**0.055**	**0.03**	**0.53**	**16.4**	**2.86**
kyx kzx kzy	0.002 0.070 0.041	-0.017 -0.037 0.003	0.031 0.0043 -0.0011	-0.001 -0.0003 -0.002	0.003 0.010 -0.008	-0.0017 -0.0 0.0002	-0.03486 0.006399 0.04281

Table 2 - Experimental and simulated results.